AV_3Sb_5 Kagome Superconductors: Progress and Future Directions

Stephen D. Wilson[1,*] **and Brenden R. Ortiz**[2,**]

[1]Materials Department, University of California Santa Barbara, California 93106, USA
[2]Materials Science and Technology Division, Oak Ridge National Laboratory, Oak Ridge, 37831, Tennessee, USA
[*]e-mail: stephendwilson@ucsb.edu
[**]e-mail: ortizbr@ornl.gov

ABSTRACT

The recent discovery of the AV_3Sb_5 (A=K, Rb, Cs) kagome superconductors launched a growing field of research investigating the interplay between superconductivity and charge density wave order in kagome metals. Specifically, the AV_3Sb_5 family naturally exhibits a Fermi level close to the Van Hove singularities associated with the saddle points formed from the prototypical kagome band structure. The charge density wave and superconducting states that form within the kagome networks of these compounds exhibit a number of anomalous properties reminiscent of theoretical predictions of exotic states in kagome metals tuned close to their Van Hove fillings. Here we provide an overview of the key structural and electronic features of AV_3Sb_5 compounds and review the status of investigations into their unconventional electronic phase transitions.

Main text

Introduction

Kagome lattices, networks of corner-sharing triangles,[1] have long been crucial building blocks for a range of unconventional states sought in condensed matter physics. Insulating compounds built from kagome networks of localized spins provide extremely rich platforms for studying magnetic frustration and spin liquid states predicted to form from the geometric frustration inherent to a kagome network.[2] Similarly, in metals, the same kagome tiling can lead to hopping interference effects[3,4] whose details depend on the position of the Fermi level relative to singularities in the electronic band structure. These interference effects along with band structures that promote strong interactions between electrons as well as topologically nontrivial electronic bands motivate study of kagome metals as hosts for an exciting new frontier of correlated topological electronic states.

Specifically, kagome networks host electronic structures that are known to exhibit bands with particle-hole asymmetric saddle points at electron fillings $f = 5/12$ and $f = 3/12$ on either side of Dirac crossings at $f = 1/3$ as well as a flat band feature.[5–7] Each of these creates a divergence in the electronic density of states at distinct momenta and energies known as a Van Hove singularity (VHS). Tuning the electron filling towards a given VHS can promote enhanced interactions between electrons and various forms of electronic order. While a form of kinetic frustration due to hopping interference leads to the formation of a localized, flat band that can promote these electron-electron interactions, similarly, fillings at the saddle points create a logarithmically divergent VHS where long-range Coulomb interactions can be promoted due to sublattice interference effects.[4] These interference effects can generate extraordinarily rich theoretical phase diagrams containing predictions of bond density wave order,[5,6] orbital magnetism,[7–9], pair density wave order,[10] topological insulator phases,[7,11] and unconventional superconductivity.[6,12–14]

Recently, considerable focus has been given to finding materials that manifest many of the unconventional electronic states predicted in kagome metals at variable fillings. This involves the identification and study of reasonably two-dimensional metals whose Fermi surfaces/low-energy properties are dominated by the electrons occupying their kagome sublattices. One focus is to identify flat band features and systematically find chemistries/perturbations that bring them toward the Fermi level. Notable recent successes observing unusual correlation effects have been reported on this front.[15–17] A second focus is to search for kagome metals possessing electron-fillings near their saddle points, similar to those sought in triangular[18] and honeycomb lattices.[19]

The VHS accessed at these saddle points generate a logarithmic divergence in the density of states at the M-points (midpoints of the edges) of the Brillouin zone (BZ), and they occur in two different flavors.[4] The first is the "p-type" VHS whose wave functions derive from a single sublattice within the three-sublattice kagome network, and the second is the "m-type" VHS comprised of wave functions mixed between sublattices. Once the filling corresponding to a VHS is reached, nest effects

between the three inequivalent M-points across the Fermi surface are predicted to promote a number of charge/spin density wave and superconducting instabilities, with the leading instability dependent on the relative importance of on-site and nearest neighbor Coulomb interactions.[6]

Materials with suitable quasi-two dimensional kagome band structures and fillings near their VHS capable of testing these predictions remained largely elusive until the discovery of the AV_3Sb_5 (A=K, Rb, Cs) class of kagome metals.[20] These compounds were first reported in 2019 as a new structure type built from a vanadium-based kagome network that forms a quasi-two dimensional structure both chemically and electronically. An important feature is that the kagome lattice of vanadium ions in AV_3Sb_5 is "nonmagnetic", meaning that the electrons on the kagome network are delocalized with no local moments (i.e. they are Pauli paramagnets).[21,22] This removes energetically favored local moment magnetism that either outcompetes or masks many of the instabilities predicted in a number of kagome lattice Hubbard models. A trivial example is the competition between static magnetic order and superconductivity or the dominant response of local moments when searching for weaker, orbital magnetism.

The goal of this review is to synthesize the experimental progress in understanding the electronic states and phase behaviors identified in the new class of AV_3Sb_5 charge density wave superconductors, where states ranging from orbital antiferromagnetism[9,23,24] to electronic nematicity[25] to pair density wave order[26] have been proposed. The key elements of the crystallographic and electronic structures of this materials class are presented first, followed by an overview of the characteristics of the high-temperature charge density wave (CDW) and the low-temperature superconducting (SC) states. The presence of intermediate energy scales or crossovers in select AV_3Sb_5 variants will be reviewed as well as the current state of experiments perturbing both CDW and SC order parameters via chemical substitution and pressure. We view the current review as timely due to the coalescence of much of the experimentally delineated phenomenology surrounding the CDW and SC order parameters in AV_3Sb_5 compounds, and we hope to help focus future measurements probing the microscopic origins of their unconventional electronic properties.

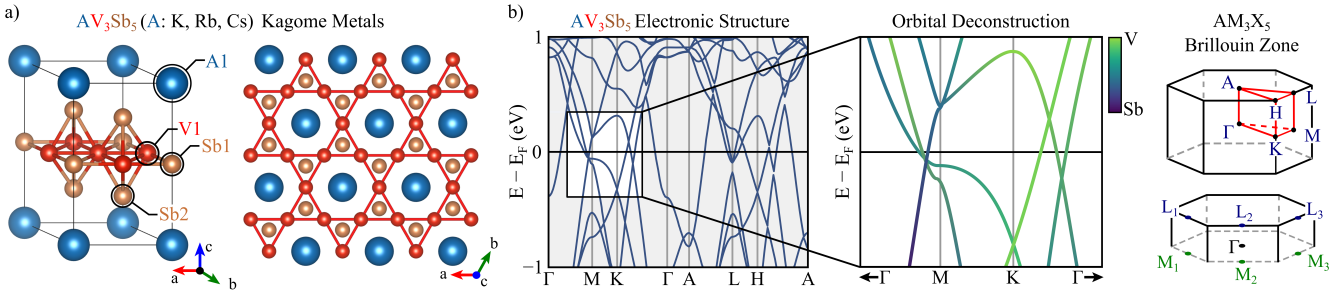

Figure 1. Crystal and electronic band structures of AV_3Sb_5 compounds a | Lattice structure of AV_3Sb_5 with A=K, Rb, Cs. Red spheres show the kagome net of V atoms, each coordinated by an octahedra of Sb atoms depicted as gold spheres. Between the V_3Sb_5 layers is a honeycomb lattice of alkali metal A-site atoms, depicted as blue spheres. b | The electronic band structure of AV_3Sb_5 determined via density functional theory calculations. Key features native to the kagome network are highlighted in the $k_z = 0$ plane such as a series of two saddle points with V orbital character just below E_F at the M-point, V-based Dirac points below E_F at the K-point, and a mixed (V,Sb) character saddle point above E_F at the M-point. A representative Brillouin zone (BZ) is also illustrated with the location of high-symmetry points labeled.

Lattice and electronic structures of AV_3Sb_5

Lattice structure

Among the highly studied kagome metal families (e.g. CoSn[27–36], $FeMn_6Ge_6$[37–46]), the AV_3Sb_5 prototype structure is distinct, as the V-Sb covalent network that forms the hallmark kagome network is intercalated by a honeycomb network of alkali metal ions. Figure 1 shows the high-temperature, undistorted crystal structure of the AV_3Sb_5 family. The orthographic perspective shows all bonds with $d < 3$ Å, highlighting the covalent V-Sb sheets and alkali intercalant. The top-down perspective shows only the V-V bonds to highlight the kagome lattice. There are two distinct sublattices of antimony in the AV_3Sb_5 system; the Sb1 sublattice within the V1 kagome sheet, and the Sb2 sublattice that forms an antimonene sublattice above and below the kagome sheets.

While many other candidate kagome metals are derivatives of the CoSn family (e.g. CoSn, $GdCo_3B_2$, $FeMn_6Ge_6$) or Laves (e.g. $MgZn_2$) prototypes, and maintain a considerable degree of three-dimensional metal-metal or covalent bonding between adjacent kagome layers, the AV_3Sb_5 structure is a unique, quasi-2D kagome structure type where the honeycomb sheets of alkali metal ions serve primarily as electron donors to the V_3Sb_5 covalent network. The alkali metal layers serve to isolate

the kagome sheets from one another, and similar motifs employing alkali, alkali-earth, and rare-earth intercalant motifs occur in the $CsCu_3S_2$,[47,48] $K_3Cu_3P_2$,[49] $Cs_2Pd_3S_4$[50], and $LnTi_3Bi_4$[51–55] families. However, many of these layered cousins suffer from more complex unit cells, orthorhombic distortions, or increased air sensitivity. The reduced dimensionality due to the alkali sublattice is critical, however, and recent computational surveys have highlighted the importance of local bonding and dimensional isolation on the potential to realize the hallmark features of a kagome metal, including the saddle points, Dirac points, and flat bands.[56]

Single crystals of AV_3Sb_5 compounds are grown via a crucible-based self-flux growth technique,[22] and typical crystal morphologies are small plates with dimensions of a few mm on each side and less than 0.5 mm thick. This volume can be scaled upward by the use of larger volume crucibles during growth where cm-scale samples can be obtained. Despite their layered structure and alkali metal content, bulk crystals are remarkably tolerant of air exposure, water, and common solvents, which increases the feasibility for a number of experimental studies. The quasi-2D nature of the AV_3Sb_5 family manifests in their mechanical properties, and single crystals are also highly exfoliable, making them well-suited for surface sensitive probes such as scanning tunneling microscopy (STM) and angle-resolved photoemission (ARPES).

The potential to control sample thickness and dimensionality via exfoliation is an avenue under exploration by the community. Experiments exploring thickness-dependent electronic properties are underway[57–60] and demonstrate that crystal thickness/confinement impacts the landscape of electronic instabilities in the AV_3Sb_5 family. Theoretical modeling of monolayer AV_3Sb_5 is consistent with this modified landscape, and suggests that monolayer samples should dramatically alter the nature of the Van Hove singularities, producing rich electronic phase diagrams.[61] Experimental efforts have been rapidly approaching monolayer samples of CsV_3Sb_5, with flakes as thin as 4 monolayers reported.[62]

Electronic structure

A schematic showing the representative band structure of AV_3Sb_5 compounds is shown in Figure 1 (b). Across the series of compounds, the band structures are qualitatively similar to one another with bands at the Fermi level dominated by the kagome nets of vanadium d-states. These are multiorbital materials with d_{xy} d_{yz} and d_{xz} derived bands forming a series of m-type and p-type VHS at the M-points of the BZ and at energies reasonably close to E_F.[63–65] Similarly, a Dirac crossing at the K-point of the BZ appears below E_F in all three compounds.

Well-defined nesting at the M-points of the Fermi surface in the $k_z = \pi$ plane was identified in ARPES measurements.[64] In CsV_3Sb_5, states identified with the m-type $d_{xz,yz}$ VHS are nearly perfectly nested and gapped below the CDW transition[64] while in KV_3Sb_5 a CDW gap was reported to open in states associated with the saddle point derived from $d_{x^2-y^2}$ V-states.[66] Optical conductivity data resolve the partial gap that opens below the CDW transition to be $\Delta_{CDW} \approx 60$ meV in KV_3Sb_5 with $T_{CDW} = 84$ K ,[67] $\Delta_{CDW} \approx 78$ meV in CsV_3Sb_5 with $T_{CDW} = 94$ K,[68] and $\Delta_{CDW} \approx 100$ meV in RbV_3Sb_5 with $T_{CDW} = 104$ K,[69]. This is notably larger than the CDW gaps estimated in some surface sensitive STM and ARPES measurements,[64,70] potentially due to matrix element and surface termination effects.[71] Other ARPES studies report CDW gaps in agreement with optical measurements[66,72], illustrative of a CDW state that forms in the strong coupling limit.

The relative importance of the multiple saddle points close to E_F remains an important area of study; in particular, whether one or multiple VHS are required to capture the essential physics of the CDW state. The ordering of the saddle points below E_F switches due to the modified (expanded) lattice of CsV_3Sb_5 relative to its K- and Rb-based cousins. In DFT models, this relative ordering VHS depends on the interlayer spacing, with KV_3Sb_5 and RbV_3Sb_5 showing a configuration with d_{xz}/d_{yz}-character VHS closest to E_F in the k_z=0 plane while CsV_3Sb_5 inverts the order with $d_{x^2-y^2}/d_{z^2}/d_{xy}$-character VHS closest to E_F.[68,73] This seemingly coincides with a unique CDW ground state in CsV_3Sb_5[74] (discussed further in the next section) and suggests that a switch in the orbital character of the Van Hove points closest to E_F impacts the favored charge instability.

We note here that electron-phonon coupling also necessarily contributes to the phase behavior in AV_3Sb_5 compounds.[75–78] DFT modeling of the lattice structure predicts a lattice instability with soft modes at the M- and L-points of the Brillouin zone,[63] and, more generally, there exists a shallow energy landscape for lattice deformation along the M-U-L line.[79] Time-resolved ARPES measurements[80] highlight the importance of the lattice degree of freedom in facilitating the CDW transition, and Raman measurements reporting hybridized lattice modes in the CDW state similarly argue for appreciable electron-phonon coupling effects.[81] The balance between these effects and purely electronic interactions driven via Fermi surface nesting remains an open area of investigation.

While the VHS arising from the kagome sublattice are important for the stabilization of CDW order, additional states at E_F originating from Sb p-orbitals likely also play a role. The large electron pocket at the Γ-point is generated by p-orbitals from the Sb sites in the kagome plane (in the centers of the hexagons of the kagome nets), and an M-point VHS of mixed Sb/V character appears slightly above E_F derived from a mixture of V-states with out-of-plane Sb p-states.[82] Doping and pressure-based studies described later in this review have shown that removal of the Γ-centered Sb band coincides with the suppression of superconductivity and that small, orbital-selective doping of the Sb bands can dramatically renormalize the CDW state. This phenomenology illustrates that both the VHS from the V d-states in the kagome sublattice as well as Sb

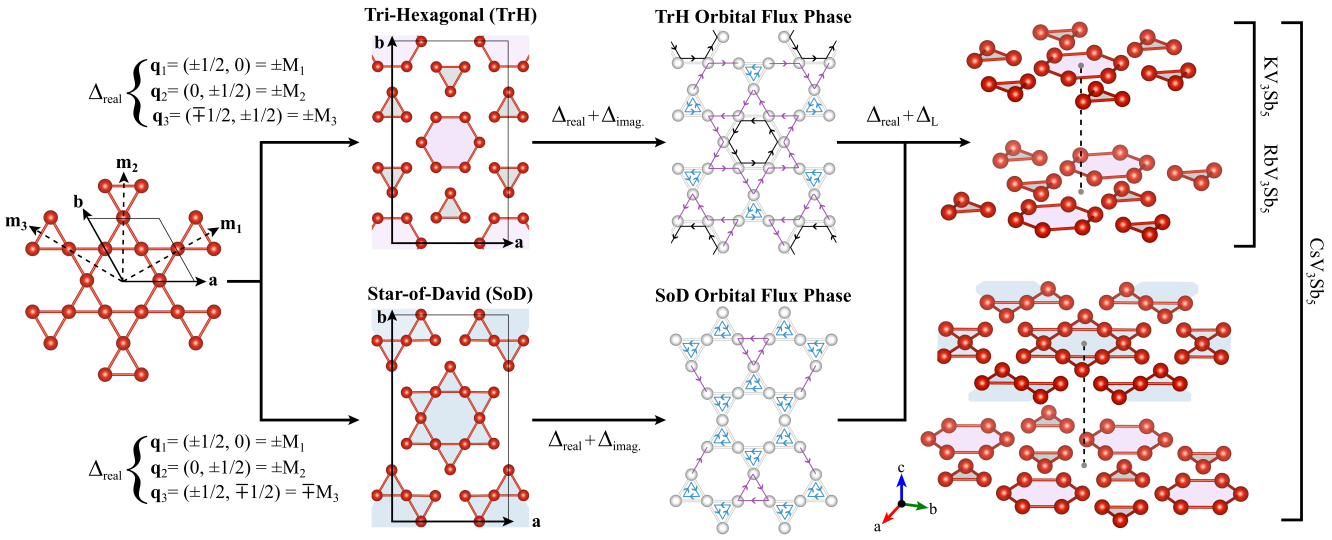

Figure 2. Elements of CDW order in AV_3Sb_5 compounds. The structure of CDW order in AV_3Sb_5 can be thought of a combination of a several key elements. The first element is the primary component of the real order parameter and is the in-plane 3**q** distortion of the kagome plane, which is favored as breathing into SoD or TrH-type distortions. The second element is the proposed imaginary component, which modulates hopping into an orbital flux phase and breaks TRS. The third element is the interplane correlation that modulates the real component of the CDW state along the *c*-axis. This arises via consideration of out-of-plane momenta (along the L-points) that modulate the phasing or distortion types between the planes. RbV_3Sb_5 and KV_3Sb_5 each show a TrH in-plane distortion that is staggered by half an in-plane lattice constant along the *c*-axis. CsV_3Sb_5 has a mixed-phase CDW, whose average 4-layer structure refines to a mixture of staggered TrH distortion interwoven with staggered TrH and SoD distorted layers.

p-states are necessary for minimal models of these compounds, where, for instance, the Sb *p*-states are proposed to mediate the three-dimensional stacking of the CDW order.[83,84]

Quantum oscillation measurements on bulk crystals confirm the quasi-two dimensional nature of the vanadium bands,[85–89] and, in the low-temperature distorted state, a number of low-frequency orbits are known to carry a non-trivial Berry phase.[86,87] Notably however, quantum oscillation measurements on micron-scale devices created from bulk crystals have been able to resolve the formation of closed 3D pockets in the CDW state at the same frequencies as those in bulk crystals, suggesting that disorder effects in bulk specimens may mask three-dimensionality in the CDW state.[90] This is consistent with ARPES measurements of ellipsoidal pockets in the CDW state[66] and with the three-dimensional nature of CDW order parameter and the expected three-dimensional zone folding. These CDW-induced orbits have small effective masses consistent with their originating from partially gapped Dirac bands centered at the K-points, and the role of these nontrivial bands in the superconducting phase remains an open question. Due to the rapid damping of quantum oscillations with increased temperature, measurements of quantum oscillations are largely confined to deep within the CDW state, and more detailed insights are often complicated by the large number of extremal orbits that appear in the reconstructed CDW state.[91]

A final, salient point regarding the band structure of AV_3Sb_5 is that there exists a continuous, direct band gap and a series of topological bands at the Fermi level. This allows for the assignment of a nontrivial $\mathbb{Z}_2$ invariant and the classification of these compounds as $\mathbb{Z}_2$ metals hosting topologically nontrivial surface states.[22] These surface states are predicted to be close to E_F[85] at the M-points, and there are experimental hints that they are pulled down to the Fermi level once the band structure is modified cooling through the CDW transition.[92] While trivial, bulk states at E_F would mask the impact of these surface states on the low-energy properties in the nonsuperconducting state, the protected surface states are potentially important within the superconducting phase where the bulk states become gapped and Fu-Kane (connate) models of topological superconductivity may apply.[93]

Charge density wave order

Real component of bond centered order

AV_3Sb_5 compounds all exhibit CDW order below T_{CDW} = 78, 104, and 94 K for A = K, Rb, and Cs respectively. Though it is difficult to resolve directly, the CDW state is predominantly modeled as deriving from bond-centered order. The main

observable is a weak structural distortion of the vanadium sublattice[22,85,94] that maps into energetically favored breathing modes of the kagome plane.[63] This distortion is accompanied by a modulation in the local density of states as imaged via STM measurements.[95–97] A number of initial experimental reports identified that the CDW state was three-dimensional with a well-defined phasing between neighboring kagome planes,[70,85,94] and the in-plane distortion can be characterized by a 3**q** breathing mode into a "Star-of-David" (SoD) or "Tri-Hexagonal" (TrH) pattern.

Both SoD and TrH patterns are supported by *ab initio* modeling, with the favored distortion modes comprised of in-plane M-point modes combined with *L*-point modes that contribute an out-of-plane modulation to the CDW structure.[63,98,99] The result is a staggering of SoD and TrH distortions along the *c*-axis by shifting each distortion pattern by half an in-plane lattice constant relative to neighboring planes. This staggering along *c* breaks the in-plane rotational symmetry and generates an orthorhombic unit cell.[74] While the relative energies of different distortion types are very close, the commonly predicted distortion mode is the staggered TrH arrangement, comprised of 3**q**=(M, L, L) modes.

The experimentally resolved CDW structures differ across the AV_3Sb_5 parent compounds. KV_3Sb_5 and RbV_3Sb_5 share a common staggered TrH distortion,[74,100,101] while CsV_3Sb_5 seemingly possesses a more complex mixture of TrH and SoD layers staggered relative to one another.[74,102–104] The average V-V distance (≈ 2.7 Å) is the same in the low-temperature charge density wave state of all three compounds, while the room temperature V-V distance expands with the alkali metal cation size. This effect combined with the different ordering of the VHS types near E_F drives a distinct pattern of CDW order in CsV_3Sb_5 marked by metastability. Specifically, the out-of-plane modulation of TrH/SoD stacking varies as a function of chemical disorder and thermal history, with regions of $2\times2\times4$ supercells competing with smaller $2\times2\times2$ supercells.[104] The formation of each of these regions is staged as a function of cooling into the CDW; however, in experiments where only $2\times2\times2$ order is isolated, a staggered TrH CDW state is observed (similar to the K- and Rb- variants).[74,103] The observation of mixed TrH and SoD order in the average structure of CsV_3Sb_5 then likely arises from the $2\times2\times4$ regions of mixed-state crystals.

Imaginary component of bond centered order

For band fillings close to a p-type VHS, an imaginary CDW state is predicted to stabilize. This is effectively a bond-centered CDW that modulates hopping across the kagome network, creating a form of orbital antiferromagnetism that breaks time-reversal symmetry (TRS). This purely orbital magnetic state exists in the absence of local spins[105] though it modifies both translational and time-reversal symmetry similar to a spin-density wave.

In AV_3Sb_5 compounds, initial hints of TRS-breaking within the CDW state were reported in STM measurements.[95,97,106] Here, a Fourier transform of the local density of states showed varying weights at the three inequivalent M-point charge superlattice peaks. The application of a magnetic field is reported to switch the relative ordering of the Fourier weights of these peaks (or the effective winding between points), suggesting a chiral CDW state that breaks TRS—an inference from the CDW coupling to an external magnetic field. While the same behavior was reported in all three AV_3Sb_5 variants, there is ongoing debate regarding the reproducibility of the effect and its origin. Separate STM studies have failed to resolve a similar magnetic field-driven switching,[107–109] and debate typically focuses on the surface conditions necessary to resolve the effect versus systematic errors in the measurement protocol. A similar debate exists in differing observations reported in optical studies. Here Kerr rotation and circular dichroism initially reported the onset of TRS breaking below the CDW transition of all three AV_3Sb_5 variants;[110] however subsequent polar Kerr measurements using a Sagnac interferometer failed to resolve net ferromagnetism or **q**=0 order.[111]

In addition to STM and optical measurements, a number of muon spin relaxation (μSR) studies suggest TRS breaking within the CDW state.[113,121,123,125] This appears in the form of an order-parameter-like modification in the muon spin relaxation rate, suggestive of the appearance of a weak, potentially inhomogenous local magnetic field. The onset of this effect appears below the CDW transition; however, in CsV_3Sb_5 and RbV_3Sb_5, there are further modifications observed at lower temperatures. Notably, the magnitude of the local field is small—comparable to nuclear moments in the sample—and traditional oscillations in the muon spin polarization, indicative of long-range magnetic order, are absent. This makes interpretation of the microscopic details driving the depolarization challenging; and interpretation of the depolarization signal as static or dynamic is proposed to be model dependent and to potentially vary between compounds.[126]

Magnetotransport measurements are another probe suggesting TRS-breaking in the CDW state. An initial measurement of a large, low-field anomalous Hall effect suggested the onset of magnetic order or spin freezing below the CDW transition in KV_3Sb_5[124], and this same effect was subsequently observed in all AV_3Sb_5 variants.[120,122] This indicates the presence of a large Berry flux generated upon entering the CDW state; however, crucially, there is no spontaneous ($\mu_0 H = 0$ T) component to the anomalous Hall response. The missing zero-field anomalous Hall response is consistent with the absence of a **q**=0 component of orbital magnetization, and magnetochiral transport studies in CsV_3Sb_5 further suggest field-switchable chirality, rooted either in the structure or broken TRS.[114] Recent torque magnetometery data[127] also report TRS-breaking albeit with an onset temperature higher than T_{CDW}, potentially reflective of the fluctuating/short-range CDW correlations reported at higher

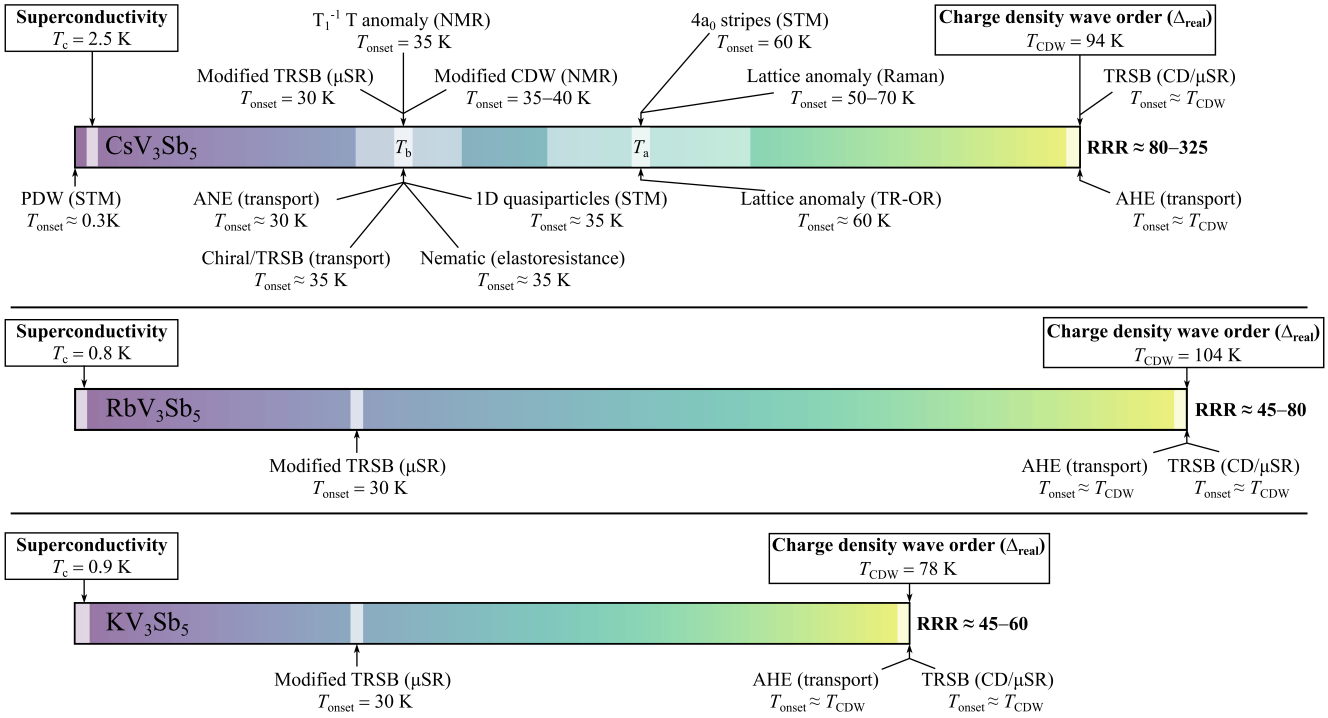

Figure 3. Intermediate electronic phase transitions and crossovers in AV_3Sb_5. The progression of phase transitions and reports of symmetry lowering, such as time reversal symmetry breaking (TRSB), in AV_3Sb_5 compounds. Reports of lattice and electronic anomalies are visually depicted here and described further in the text. The range of reported residual resistivity ratios (RRR $\equiv \rho_{4K}/\rho_{300K}$) for each compound is summarized next to each chart of anomalies. The majority of anomalies intermediate between the onset of CDW order and SC are currently reported in CsV_3Sb_5. Data for CsV_3Sb_5 are drawn from PDW[26], ANE[112], Modified TRSB (μSR)[113], Chiral/TRSB (transport)[114], 1D quasiparticles (STM)[108], Nematic (elastoresistance)[115], Modified CDW (NMR)[116], $T^{-1}T$ anomaly (NMR)[117], $4a_0$ stripes (STM)[96], Lattice anomaly (Raman)[79,118], Lattice anomaly (TR-OR)[119], AHE[120], TRSB (CD)[110], and TRSB (μSR)[116]. Data for RbV_3Sb_5 are drawn from TRSB (CD)[110], TRSB (μSR)[121], AHE[122], and modified TRSB (μSR)[121]. Data for KV_3Sb_5 are drawn from TRSB (CD)[110], TRSB (μSR)[123], AHE[124], and modified TRSB (μSR)[123].

temperatures in this compound.[128,129]

Staged electronic order

A further signature of the unconventional nature of CDW order in AV_3Sb_5 compounds is the appearance of a number of intermediate crossover behaviors that appear upon cooling toward the SC state. Figure 3 illustrates the temperature scales of these anomalies, suggesting a staged evolution of electronic order upon cooling. The vast majority of these reports are reported in CsV_3Sb_5, with only muon spectroscopy reporting intermediate states in the RbV_3Sb_5 and KV_3Sb_5 compounds.

This difference between compounds likely stems from one of two origins. The first is that the crystal quality of CsV_3Sb_5 is typically superior to that of the other variants, with residual resistivity ratios (RRR) reported as high as 300 (compared to RRR=60-80 reported in the Rb- and K-variants).[89,112,130] This engenders greater exploration by the community, and the lower disorder potentially stabilizes or unmasks subtle experimental signatures of crossover regimes in the CDW state. In this scenario, staging of the electronic order is naively present in all three AV_3Sb_5 compounds, but it remains hidden in less frequently studied crystals with poorer quality.

The second possibility is that the subtly different band structure of CsV_3Sb_5 and the change in the relative ordering of VHS close to E_F generates this crossover behavior. This scenario would imply that the distinct pattern of CDW order and metastability that CsV_3Sb_5 realizes creates a distinct thermal evolution of the CDW state upon cooling. As will be discussed later, CsV_3Sb_5 also possesses distinct doping- and pressure-tuned phase diagrams, suggesting the this second scenario of a unique starting CDW state is the most likely origin for its richer thermal evolution of electronic states.

Focusing on CsV_3Sb_5, a number of experimental probes report signatures of either lattice or electronic anomalies near

$T_a \approx 60$ K and $T_b \approx 35$ K as summarized in the top panel of Figure 3. Each of these temperature scales lacks a sharp thermodynamic anomaly in the heat capacity, suggesting they originate from a subtle crossover in the electronic structure. The first anomaly T_a is defined primarily by the emergence of a short-lifetime phonon mode in optics measurements,[79,118,119] suggesting that it is coupling to an electronic degree of freedom. T_a also coincides with the appearance of quasi-one dimensional charge stripes with a real space lattice modulation of four lattice constants ($4a_0$) on the surface resolved by STM studies.[96]

Upon further cooling, a second energy scale appears at T_b. This energy scale is characterized by probes reporting rotational symmetry breaking and higher harmonics in magnetotransport, suggestive of the onset of chirality or TRS breaking.[112,114,115,117] Notably, T_b also coincides with the onset of quasi-one dimensional band features in quasi-particle interference spectra[108] as well as a modification in the local Sb environment[116] and changes in the local magnetic field detected in muon spin relaxation studies.[113] One potential interpretation is that the T_a energy scale represents the onset of emergent CDW fluctuations that couple to the lattice and slowly freeze toward T_b, affecting a crossover in the electronic structure and transport properties.

A candidate origin of the staged behavior within the CDW state is the CDW-driven nesting of small pockets in the folded BZ following the onset of CDW order. Figure 4 (a) illustrates this scenario where the nested VHS at the M-points in the folded, $P6/mmm$ cell reconstruct the zone via a TrH distortion into a smaller BZ. The reconstructed zone possesses small pockets that nest along a new $\mathbf{q}=\frac{3}{2}\mathrm{M}$ (and equivalent wave vectors) and can drive a secondary instability at lower temperature.[131] These small pockets were recently observed in a joint STM and ARPES study, and they are proposed to be Chern pockets that support nesting for a new $3\mathbf{q}$-type order with a real space modulation of $(4a_0/3)$.[132]

The emergent, new $3\mathbf{q}$ wave vector corresponds to the anomalous charge correlations that appear at low-temperature and modulate the superfluid density at the surface as reported in scanning Josephson tunneling measurements.[26] This observation has invoked the notion of an intertwined CDW and SC state connected through a primary pair density wave instability.[10] How ubiquitous this phenomenon is in other AV_3Sb_5 compounds, and whether the emergent $4a_0/3$-type correlations arise from the nearby T_b energy scale remains to be established. Figure 4 (b) summarizes the reports of local charge correlations present in the different material classes and their visualization in STM measurements.

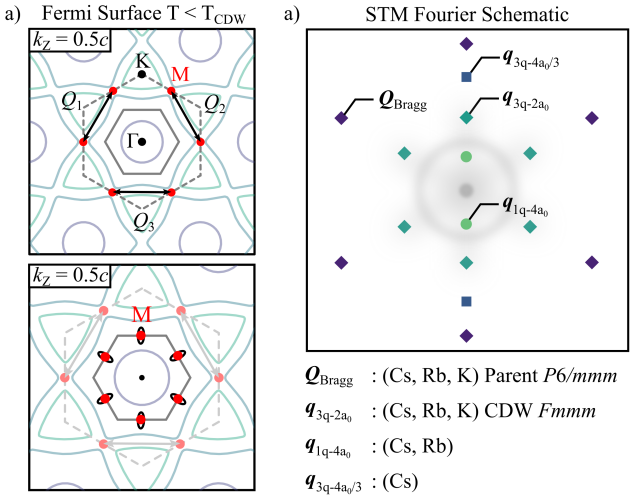

Figure 4. Schematic of momentum space contours of the Fermi surface and corresponding nesting wave vectors for electronic order. a | Nesting wave vectors in the unfolded and folded BZ above and below the CDW transition respectively. Nested M-points are illustrated in the unfolded zone while a schematic of nested Chern pockets are highlighted in the folded zone, below T_{CDW}. b | Wave vectors of charge correlations resolved within the ab-plane as reported via STM measurements and a tabulation of compounds where these correlations have been reported.

Superconducting order

All three parent AV_3Sb_5 compounds host a superconducting transition within the CDW state, with the highest $T_c = 2.5$ K in CsV_3Sb_5[22] and $T_c \approx 0.9$ K for $(Rb,K)V_3Sb_5$.[133,134] Note that the precise T_c reported for each compound varies somewhat between experimental reports (some higher and some lower by a few hundred mK). Due to the competition between SC and the CDW states under slight doping, vetting the "correct" T_c requires detailed parametrization of the CDW state in the same sample. The SC state forms in the clean limit with $l >> \xi_{ab}$ (where l is the mean free path and ξ is the coherence length),[135] and the SC state is highly anisotropic with a critical field ratio $H_{c2,ab}/H_{c2,c} \approx 9$.[136]

One of the main challenges in studies of AV_3Sb_5 compounds is to conclusively define the pairing symmetry of the SC order parameter. Despite a number of initially mixed results reporting nodeless versus nodal SC order parameters, the experimental picture has slowly converged to a nodeless,[135,137] anisotropic[138] SC gap function with singlet pairing[139]. A multiband, two gap SC state manifests where one gap is substantially smaller than the other[140,141]—making conventional assessment of low-temperature thermal transport and "U"- versus "V"-shaped SC gap spectra in STM challenging due to quasiparticle contamination from the lower gap. The lower gap size determined via penetration depth measurements is estimated to be

$\Delta_{small} \approx 0.5\ k_B T_c$[135,138] while the larger gap from tunneling measurements is estimated to range between $\Delta_{large} \approx 2.5 - 3.6\ k_B T_c$.[26,140] This is also consistent with a model of two-gap s-wave model utilized in a μsR study.[126]

A number of different types of SC are predicted to emerge due to nested VHS in the kagome band structure. A leading instability in many models is for a chiral $d + id$ SC state to emerge.[4] Such a state would be consistent with the observation of a nodeless SC gap function and reports of broken TRS in the superconducting state;[121] however recent irridation-based studies of the response of the SC gap to disorder suggest that such a state can be precluded (as well as sign changing $s^{\pm}$).[138] This assessment is based on a conventional picture of a sign-changing gap function being more sensitive to lattice disorder; however recent theoretical models of SC on the kagome lattice suggest that this conventional assumption may not be valid.[142] Specifically, the sublattice character of the kagome network near Van Hove fillings renders disorder to be non-pairing breaking for singlet pairing mechanisms irregardless of whether there is a sign change in the gap function. Future work exploring this idea and whether $d + id$ pairing can truly be precluded from existing results is merited.

Upon warming outside of the saturated SC state, additional anomalies are reported near T_c. Recent mutual inductance measurements report an extended vortex liquid regime in CsV_3Sb_5[143], suggesting that an unconventional fluctuation regime may be present. 6e pairing states are predicted to stabilize in such a fluctuation regime in the presence of orbital antiferromagnetism.[144] While Little-Parks measurements probing magnetoresistance oscillations in SC ring devices indeed report an evolution from 2e- to 4e- to 6e-pairing upon warming through the SC transition[145], these measurements have yet to be replicated and potential spurious origins for this effect are debated.

Interplay between superconductivity and charge density wave order

The local interplay between charge correlations and the SC state is most extensively visualized in STM measurements, where, at least at the surface and excluding the emergent $\mathbf{q}=\frac{3}{2}$-type wave vector, there is smooth coexistence of 2×2-type charge correlations and the SC gap. Perturbing the CDW state via external pressure or chemical doping, however, can have a dramatic effect on the SC phase, which we summarize below.

As alluded to earlier in this review, the pressure and doping responses of KV_3Sb_5 and RbV_3Sb_5 differ from those of CsV_3Sb_5. For (K, Rb)V_3Sb_5, the application of hydrostatic pressure rapidly suppresses T_{CDW} while simultaneously enhancing T_c.[147,148] The left hand side of Figure 5 (a) shows this common response as the normalized CDW transition temperature for both compounds follows a similar pressure dependence normalized for the critical pressure (P_c) necessary to destabilize CDW order.

In both compounds, the suppression of the CDW state eventually terminates in a first-order line where T_c is maximized. The evolution of the SC state up to and across P_c is nearly identical, and a maximal $T_c = 4$ K is realized for both materials as CDW order is suppressed. While a conventional picture of the trade-off between T_{CDW} and T_c is that pressure naively pushes the Fermi level away from the two occupied VHS closest to E_F (as shown in the inset of Figure 5 (a)[73]), destabilizing CDW order and enhancing SC via an increased density of states, the details of the trade-off between the two states differs somewhat from this simple picture. In particular, T_c is maximized within the CDW state for RbV_3Sb_5 where the suppression of the CDW state is tracked more fully. This likely reflects the impact of additional modifications to the band structure (in particular to the Sb p-states) in tandem to a destabilization of the CDW order parameter.

On the right hand side of Figure 5 (a), a distinct pressure-induced response of CsV_3Sb_5 is shown using the normalized critical pressure and CDW onset temperatures.[146,151] Pressure again drives a rapid suppression of CDW order that terminates in a first-order line; however T_c evolves in a nonmonotonic manner, forming two SC "domes" within the (P, T) phase diagram. The first dome reaches a peak T_c *within* the long-range ordered CDW region of the phase diagram. With continued increasing pressure, the CDW is monotonically suppressed, yet T_c decreases to close to its zero-pressure value before increasing again to a global maximum near the first-order CDW phase boundary. Moving beyond this boundary with increasing pressure causes T_c to decrease again and form a second, extended "dome". The termination of the second, higher pressure SC dome seemingly correlates with the removal from the Fermi surface of the Sb p_z states forming the electron-like pocket centered at the Γ-point of the BZ.[152] The lower pressure dome, in contrast, is likely driven by a CDW transition where charge correlations are weakened as they evolve out of the distinct, parent CDW order in CsV_3Sb_5 into an incommensurate charge density wave state,[153,154] and partial volume fraction SC is reported near this phase boundary.

Tuning the electron-filling (and thus the Fermi level alignment with the VHS) is another means of studying the interplay between the CDW order and its coupling to the SC state. Figure 5 (b) shows the normalized CDW transitions for all three parent compounds as a function of critical concentrations of hole-doping x_c where x is the number of doped holes per formula unit. As shown in the inset, hole-doping is naively expected to shift the Fermi level closer to occupied VHS in the band structure, though in an orbitally selective manner with the major changes expected in the filling of the Sb-derived Γ-pocket.[73,149] Again, the relative responses of (K, Rb)V_3Sb_5 and CsV_3Sb_5 are distinct.

Looking first at the left side of Figure 5 (b), hole-doping drives a rapid suppression of CDW order in (K, Rb)V_3Sb_5, resulting in a common enhancement in T_c up to 4 K.[150] On the right hand side of the plot, CsV_3Sb_5 again shows a double-dome-type

evolution where T_c first reaches a maximum *inside* the CDW state followed by a minimum just beyond the first-order phase boundary where CDW order vanishes.[149] Continued hole-doping drives an increase in T_c to a second maximum outside of the CDW state near $x \approx 0.33$. While not shown in Figure 5 (b), continued hole-doping then drives a slight decrease in T_c before SC vanishes in the second dome near $x \approx 0.7$. Again, SC vanishes near the doping concentration where the Sb-derived Γ-pocket is predicted to be lifted above E_F in DFT calculations. These phase diagrams can be most extensively mapped using Sn-atoms as hole-dopants replacing Sb, and qualitatively similar phase diagrams form using Ti-atoms as dopants replacing V,[155,156] albeit with lower solubility limits and stronger disorder effects.

There are clear commonalities in the (P,T) and (x, T) phase diagrams. For instance, the rapid suppression of the CDW state for all compounds as a function of pressure and hole-doping is uniformly observed and anomalous, in particular given the differing effects on proximities of the VHS to E_F for the two different types of perturbations. The differing response of SC to the suppression of CDW order between CsV_3Sb_5 and (K,Rb)V_3Sb_5 using both types of perturbations likely arises from the unique starting CDW phase of CsV_3Sb_5. The charge correlations in the seemingly metastable starting CDW state of CsV_3Sb_5 change in character under small perturbations, creating strong charge fluctuations as they evolve. The phase boundary or crossover out of the metastable starting CDW state is one possible origin for the initial low-pressure/low-doping dome in CsV_3Sb_5.

Incommensurate quasi-one dimensional charge correlations were recently observed near the CDW phase boundary of hole-doped CsV_3Sb_5 suggesting such a crossover may exist.[157] NMR measurements similarly report the presence of incommensurate charge correlations near the boundary between pressure-driven SC domes in this material.[154] Whether or not similar incommensurate charge correlations emerge beyond the CDW phase boundaries of (K,Rb)V_3Sb_5, however, has yet to be explored. A second commonality in the pressure/doping phase diagrams of CsV_3Sb_5 is the complete suppression of SC once the Sb p_z states are driven away from E_F, suggesting that these states remain essential to stabilizing SC. Furthermore, given that the primary effect on the band structure of both hydrostatic pressure and hole-doping is an orbitally selective modification of the Sb Γ-pocket, the rapid suppression of CDW order in both phase diagrams suggests that the Sb states are intertwined with the V-atom driven CDW order in an unconventional manner. Resonant x-ray scattering measurements have further resolved that Sb states are coupled/hybridized within the CDW transition[158] despite minimal motion of Sb sites through T_{CDW}.

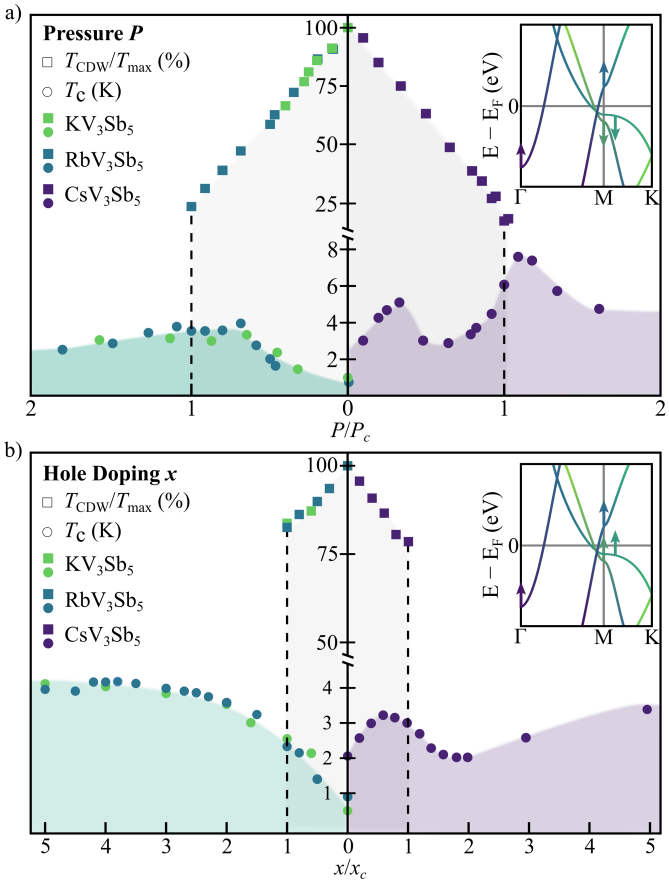

Figure 5. Doping and pressure-tuned phase diagrams of AV_3Sb_5 compounds. a | Pressure-Temperature electronic phase diagram showing the evolution of CDW and SC orders as a function of normalized pressure. The pressure value is normalized by the critical pressure P_c where the CDW state is reported to vanish. b | Electronic phase diagram as a function of normalized hole-doping. Doping concentrations have been normalized by the critical hole-doping value x_c where CDW order nominally vanishes. CDW transition temperatures have been normalized relative to their undoped, ambient pressure values of 100%. Data were adapted from[146–150].

Outlook/Future Perspectives

A number of recent studies have probed the chemical flexibility of AV_3Sb_5 compounds both in terms of filling control and in terms of isoelectronic/steric perturbation.[156,159–171] A survey of various chemical substitutions reported and the corresponding changes to T_{CDW} and T_c for CsV_3Sb_5 is summarized in Figure 6. We only list results from single crystal studies where disorder effects tend to be smaller. Generally speaking, solubility limits for chemical substitution seem largest in CsV_3Sb_5, and by far the most research continues to be invested into the Cs-variant of the structure. Site substitution is possible to varying degrees on all sites in the lattice, and this provides a valuable litmus for testing the essential band features and interactions necessary for stabilizing the various types of

electronic order in these compounds.

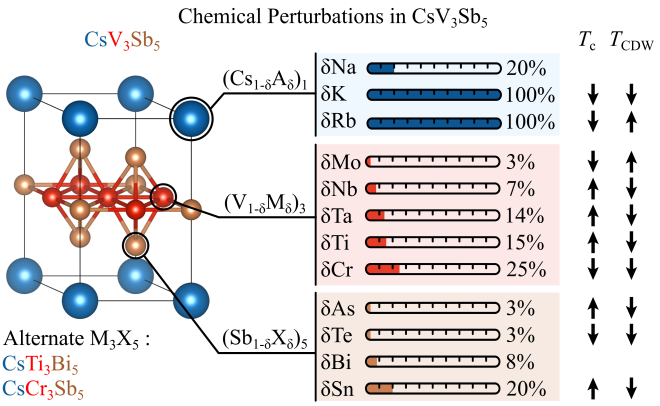

Figure 6. Schematic showing sublattice doping of CsV_3Sb_5 with various electronic, magnetic, and isoelectronic dopants. Percent substitution achievable for dopants on each site of CsV_3Sb_5 and their influence on T_{CDW} and T_c are illustrated. Data are extracted from[156, 159–171]

Crucially, new parent systems with the same structure type have also been discovered, providing a platform for exploring the impact of forming the same kagome lattice at different fillings. For instance, the recently reported Ti-based variants (Rb,Cs)Ti_3Bi_5 possess a dramatically different band structure and no signatures of CDW order.[172–174] There are however reports of an intrinsic rotational symmetry breaking in the quasiparticle spectra of these compounds, suggesting an underlying nematic electronic instability and continued correlation effects.[175] At lower temperatures, superconductivity was reported in $CsTi_3Bi_5$, though there exists a debate whether the SC state is intrinsic or arises from an impurity phase.[172, 176] A new Cr-based variant $CsCr_3Sb_5$ was also very recently reported with a complex evolution of charge order and potential coexisting, local moment magnetic order.[177] These are exciting developments and suggest further unconventional states can be realized via engineering added interactions across the kagome network of the AM_3X_5 structure-type.

In order to understand the origin of the anomalous properties in AV_3Sb_5, the role of the seemingly nested VHS at E_F in driving the staged phase behavior needs to be further constrained experimentally, and the band features necessary for a minimal model of their properties need to be determined. In particular, the relative importance of the in-plane and out-of-plane Sb p-states in stabilizing CDW order, SC, or both is an important open question. Other material comparators with similar band fillings may provide clues to this. For instance, kagome net RV_6Sn_6 compounds (R=rare earth), while more three-dimensional, possess similar VHS near their Fermi levels, yet they lack similar phase electronic phase transitions.[178, 179] A crucial difference is likely that the Sn sites are pushed out of the V-based kagome nets, removing a comparable Sn p-pocket at the Γ-point in the BZ.

Going forward, crucial experiments directly resolving the symmetries broken in the CDW state of AV_3Sb_5 are either planned or underway. Whether or not TRS is broken via a bond-centered CDW is a central question and, if confirmed, would represent the first manifestation of orbital antiferromagnetism in the solid state. One likely resolution to experimental discrepancies in resolving a TRS-broken state is the impact of strain on the response of AV_3Sb_5 compounds. While an externally applied, in-plane strain field has a muted impact on the relative T_c and T_{CDW} values (likely driven via the Poisson ratio),[180], strain fields either frozen within crystals or imparted during mounting/cooling samples have recently been shown to have a dramatic impact on the electronic responses associated with broken TRS and rotational symmetry breaking.

Specifically, removal/minimization of strain fields within crystals of CsV_3Sb_5 seemingly governs whether rotational symmetry breaking is observable within in-plane charge transport measurements.[181] Furthermore, an applied magnetic field orthogonal to the kagome planes induces in-plane transport anisotropy, suggestive of a piezomagnetic response and a natural coupling of TRS-breaking order to strain. Recent STM measurements directly resolve such a piezomagnetic response as well as optically-induced switching of chirality in the CDW state at the surface of RbV_3Sb_5 crystals.[182] The emerging picture is then one of a native orbital antiferromagnetic state that breaks TRS and is strongly coupled to out-of-plane magnetic fields and in-plane strain fields.[183] These fields can imbalance the components of the multi-q CDW order and induce a net ferromagnetic or **q**=0 signal detectable by a number of probes (such as Kerr rotation measurements). Future work exploring the notion of strain's impact on the weak magnetic signal detected in muon spin relaxation and optics measurements is an exciting path forward.

Resolving the above puzzles will provide crucial hints for the pairing symmetry of the lower temperature superconducting state in AV_3Sb_5 compounds and hopefully motivate the search for new materials platforms that host similar band structures. The number of new AM_3X_5 variants recently uncovered is a promising new direction for exploring other correlated states possible on a kagome network. We envision many new opportunities will emerge as this new materials phase space is fully explored and the rich frontier of states predicted within kagome metals can be tested in real material platforms.

Author contributions

S.D.W. and B.R.O. composed the manuscript and created the figures.

References

1. Syôzi, I. Statistics of kagomé lattice. *Prog. Theor. Phys.* **6**, 306–308 (1951).
2. Norman, M. Colloquium: Herbertsmithite and the search for the quantum spin liquid. *Rev. Mod. Phys.* **88**, 041002 (2016).
3. Bergman, D. L., Wu, C. & Balents, L. Band touching from real-space topology in frustrated hopping models. *Phys. Rev. B* **78**, 125104, DOI: 10.1103/PhysRevB.78.125104 (2008).
4. Kiesel, M. L. & Thomale, R. Sublattice interference in the kagome hubbard model. *Phys. Rev. B* **86**, 121105 (2012).
5. Wang, W.-S., Li, Z.-Z., Xiang, Y.-Y. & Wang, Q.-H. Competing electronic orders on kagome lattices at van hove filling. *Phys. Rev. B* **87**, 115135 (2013).
6. Kiesel, M. L., Platt, C. & Thomale, R. Unconventional fermi surface instabilities in the kagome hubbard model. *Phys. review letters* **110**, 126405 (2013).
7. Wen, J., Rüegg, A., Wang, C.-C. J. & Fiete, G. A. Interaction-driven topological insulators on the kagome and the decorated honeycomb lattices. *Phys. Rev. B* **82**, 075125 (2010).
8. Nayak, C. Density-wave states of nonzero angular momentum. *Phys. Rev. B* **62**, 4880–4889, DOI: 10.1103/PhysRevB.62.4880 (2000).
9. Lin, Y.-P. & Nandkishore, R. M. Complex charge density waves at Van Hove singularity on hexagonal lattices: Haldane-model phase diagram and potential realization in the kagome metals AV_3Sb_5 (A= K, Rb, Cs). *Phys. Rev. B* **104**, 045122 (2021).
10. Wu, Y.-M., Thomale, R. & Raghu, S. Sublattice interference promotes pair density wave order in kagome metals. *Phys. Rev. B* **108**, L081117 (2023).
11. Guo, H.-M. & Franz, M. Topological insulator on the kagome lattice. *Phys. Rev. B* **80**, 113102, DOI: 10.1103/PhysRevB.80.113102 (2009).
12. Yu, S.-L. & Li, J.-X. Chiral superconducting phase and chiral spin-density-wave phase in a hubbard model on the kagome lattice. *Phys. Rev. B* **85**, 144402, DOI: 10.1103/PhysRevB.85.144402 (2012).
13. Wu, X. *et al.* Nature of Unconventional Pairing in the Kagome Superconductors AV_3Sb_5 (A=K,Rb,Cs). *Phys. Rev. Lett.* **127**, 177001, DOI: 10.1103/PhysRevLett.127.177001 (2021).
14. Lin, Y.-P. & Nandkishore, R. M. Multidome superconductivity in charge density wave kagome metals. *Phys. Rev. B* **106**, L060507, DOI: 10.1103/PhysRevB.106.L060507 (2022).
15. Kang, M. *et al.* Topological flat bands in frustrated kagome lattice cosn. *Nat. communications* **11**, 4004 (2020).
16. Ye, L. *et al.* A flat band-induced correlated kagome metal. *arXiv:2106.10824* (2021).
17. Huang, H. *et al.* Flat-band-induced anomalous anisotropic charge transport and orbital magnetism in kagome metal cosn. *Phys. Rev. Lett.* **128**, 096601, DOI: 10.1103/PhysRevLett.128.096601 (2022).
18. Martin, I. & Batista, C. D. Itinerant electron-driven chiral magnetic ordering and spontaneous quantum hall effect in triangular lattice models. *Phys. Rev. Lett.* **101**, 156402, DOI: 10.1103/PhysRevLett.101.156402 (2008).
19. Nandkishore, R., Levitov, L. S. & Chubukov, A. V. Chiral superconductivity from repulsive interactions in doped graphene. *Nat. Phys.* **8**, 158–163, DOI: 10.1038/nphys2208 (2012).
20. Ortiz, B. R. *et al.* New kagome prototype materials: discovery of KV_3Sb_5, RbV_3Sb_5, and CsV_3Sb_5. *Phys. Rev. Mater.* **3**, 094407, DOI: 10.1103/PhysRevMaterials.3.094407 (2019).
21. Kenney, E. M., Ortiz, B. R., Wang, C., Wilson, S. D. & Graf, M. J. Absence of local moments in the kagome metal KV_3Sb_5 as determined by muon spin spectroscopy. *J. Physics: Condens. Matter* **33**, 235801 (2021).
22. Ortiz, B. R. *et al.* CsV_3Sb_5: A Z2 Topological Kagome Metal with a Superconducting Ground State. *Phys. Rev. Lett.* **125**, 247002, DOI: 10.1103/PhysRevLett.125.247002 (2020).
23. Feng, X., Zhang, Y., Jiang, K. & Hu, J. Low-energy effective theory and symmetry classification of flux phases on the kagome lattice. *Phys. Rev. B* **104**, 165136, DOI: 10.1103/PhysRevB.104.165136 (2021).
24. Denner, M. M., Thomale, R. & Neupert, T. Analysis of Charge Order in the Kagome Metal AV_3Sb_5 (A=K,Rb,Cs). *Phys. Rev. Lett.* **127**, 217601, DOI: 10.1103/PhysRevLett.127.217601 (2021).
25. Grandi, F., Consiglio, A., Sentef, M. A., Thomale, R. & Kennes, D. M. Theory of nematic charge orders in kagome metals. *Phys. Rev. B* **107**, 155131, DOI: 10.1103/PhysRevB.107.155131 (2023).

26. Chen, H. *et al.* Roton pair density wave in a strong-coupling kagome superconductor. *Nature* **599**, 222–228 (2021).

27. Yu, X. *et al.* Near room-temperature formation of a skyrmion crystal in thin-films of the helimagnet FeGe. *Nat. materials* **10**, 106–109 (2011).

28. Xie, Y. *et al.* Spin excitations in metallic kagome lattice FeSn and CoSn. *Commun. Phys.* **4**, 240 (2021).

29. Bak, P. & Jensen, M. H. Theory of helical magnetic structures and phase transitions in MnSi and FeGe. *J. Phys. C: Solid State Phys.* **13**, L881 (1980).

30. Kang, M. *et al.* Dirac fermions and flat bands in the ideal kagome metal FeSn. *Nat. materials* **19**, 163–169 (2020).

31. Meier, W. R. *et al.* Flat bands in the CoSn-type compounds. *Phys. Rev. B* **102**, 075148 (2020).

32. Liu, Z. *et al.* Orbital-selective Dirac fermions and extremely flat bands in frustrated kagome-lattice metal CoSn. *Nat. communications* **11**, 4002 (2020).

33. Sales, B. *et al.* Tuning the flat bands of the kagome metal CoSn with Fe, In, or Ni doping. *Phys. Rev. Mater.* **5**, 044202 (2021).

34. Teng, X. *et al.* Magnetism and charge density wave order in kagome FeGe. *Nat. Phys.* 1–9 (2023).

35. Kang, M. *et al.* Topological flat bands in frustrated kagome lattice CoSn. *Nat. communications* **11**, 4004 (2020).

36. Sales, B. C. *et al.* Electronic, magnetic, and thermodynamic properties of the kagome layer compound FeSn. *Phys. Rev. Mater.* **3**, 114203 (2019).

37. Arachchige, H. W. S. *et al.* Charge Density Wave in Kagome Lattice Intermetallic ScV_6Sn_6. *Phys. Rev. Lett.* **129**, 216402 (2022).

38. El Idrissi, B. C., Venturini, G., Malaman, B. & Fruchart, D. Magnetic structures of $TbMn_6Sn_6$ and $HoMn_6Sn_6$ compounds from neutron diffraction study. *J. Less Common Met.* **175**, 143–154 (1991).

39. Ghimire, N. J. *et al.* Competing magnetic phases and fluctuation-driven scalar spin chirality in the kagome metal YMn_6Sn_6. *Sci. Adv.* **6**, eabe2680 (2020).

40. Lee, J. & Mun, E. Anisotropic magnetic property of single crystals RV_6Sn_6 (R= Y, Gd- Tm, Lu). *Phys. Rev. Mater.* **6**, 083401 (2022).

41. Peng, S. *et al.* Realizing Kagome Band Structure in Two-Dimensional Kagome Surface States of RV_6Sn_6 (R= Gd, Ho). *Phys. review letters* **127**, 266401 (2021).

42. Pokharel, G. *et al.* Electronic properties of the topological kagome metals YV_6Sn_6 and GdV_6Sn_6. *Phys. Rev. B* **104**, 235139 (2021).

43. Pokharel, G. *et al.* Highly anisotropic magnetism in the vanadium-based kagome metal TbV_6Sn_6. *Phys. Rev. Mater.* **6**, 104202 (2022).

44. Wang, Q. *et al.* Field-induced topological Hall effect and double-fan spin structure with a c-axis component in the metallic kagome antiferromagnetic compound YMn_6Sn_6. *Phys. Rev. B* **103**, 014416 (2021).

45. Yin, J.-X. *et al.* Quantum-limit Chern topological magnetism in $TbMn_6Sn_6$. *Nature* **583**, 533–536 (2020).

46. Zhang, X. *et al.* Electronic and magnetic properties of intermetallic kagome magnets RV_6Sn_6 (R= Tb- Tm). *Phys. Rev. Mater.* **6**, 105001 (2022).

47. Klepp, K. & Weithaler, C. The crystal structures of $CsAu_3S_2$, $RbAu_3Se_2$ and $CsAu_3Se_2$ and their relationship to the $CsCu_3S_2$ structure type. *J. alloys compounds* **243**, 1–5 (1996).

48. Burschka, C. $CsCu_4S_3$ und $CsCu_3S_2$: Sulfide mit tetraedrisch und linear koordiniertem Kupfer. *Z. anorg. allg. Ohem.* **483**, 65–71 (1980).

49. Savelsberg, G. & SCHAFER, H. Darstellung und Kristallstruktur von $K_3Cu_3P_2$. *Z. Naturforsch. B* **33**, 590–592 (1978).

50. Bronger, W. & Huster, J. $Cs_2Pd_3S_4$, ein neuer schichtenstrukturtyp. *J. Less Common Met.* **23**, 67–72 (1971).

51. Ortiz, B. R. *et al.* YbV_3Sb_4 and EuV_3Sb_4 vanadium-based kagome metals with Yb^{2+} and Eu^{2+} zigzag chains. *Phys. Rev. Mater.* **7**, 064201, DOI: 10.1103/PhysRevMaterials.7.064201 (2023).

52. Ortiz, B. R. *et al.* Evolution of Highly Anisotropic Magnetism in the Titanium-Based Kagome Metals $LnTi_3Bi_4$ (Ln: La··· Gd^{3+}, Eu^{2+}, Yb^{2+}). *Chem. Mater.* **35**, 9756–9773 (2023).

53. Ovchinnikov, A. & Bobev, S. Synthesis, Crystal and Electronic Structure of the Titanium Bismuthides $Sr_5Ti_{12}Bi_{19+x}$, $Ba_5Ti_{12}Bi_{19+x}$, and $Sr_{5-\delta}Eu_\delta Ti_{12}Bi_{19+x}$ (x=0.5–1.0; δ=2.4, 4.0). *Eur. J. Inorg. Chem.* **2018**, 1266–1274 (2018).

54. Ovchinnikov, A. & Bobev, S. Bismuth as a reactive solvent in the synthesis of multicomponent transition-metal-bearing bismuthides. *Inorg. Chem.* **59**, 3459–3470 (2019).

55. Motoyama, G. *et al.* Magnetic properties of new antiferromagnetic heavy-fermion compounds, Ce_3TiBi_5 and $CeTi_3Bi_4$. *Phys. B Condens.* **536**, 142–144 (2018).

56. Jovanovic, M. & Schoop, L. M. Simple chemical rules for predicting band structures of kagome materials. *J. Am. Chem. Soc.* **144**, 10978–10991 (2022).

57. Song, B. *et al.* Anomalous enhancement of charge density wave in kagome superconductor csv_3sb_5 approaching the 2d limit. *Nat. Commun.* **14**, 2492 (2023).

58. Wei, X. *et al.* Linear nonsaturating magnetoresistance in kagome superconductor thin flakes. *2D Mater.* **10**, 015010 (2022).

59. Wu, Y. *et al.* Nonreciprocal charge transport in topological kagome superconductor CsV_3Sb_5. *npj Quantum Mater.* **7**, 105 (2022).

60. Wang, T. *et al.* Enhancement of the superconductivity and quantum metallic state in the thin film of superconducting Kagome metal KV_3Sb_5. *arXiv preprint arXiv:2105.07732* (2021).

61. Kim, S.-W., Oh, H., Moon, E.-G. & Kim, Y. Monolayer Kagome metals AV_3Sb_5. *Nat. Commun.* **14**, 591 (2023).

62. Song, Y. *et al.* Competition of superconductivity and charge density wave in selective oxidized CsV_3Sb_5 thin flakes. *Phys. review letters* **127**, 237001 (2021).

63. Tan, H., Liu, Y., Wang, Z. & Yan, B. Charge density waves and electronic properties of superconducting kagome metals. *Phys. Rev. Lett.* **127**, 046401, DOI: 10.1103/PhysRevLett.127.046401 (2021).

64. Kang, M. *et al.* Twofold van Hove singularity and origin of charge order in topological kagome superconductor CsV_3Sb_5. *Nat. Phys.* **18**, 301–308 (2022).

65. Hu, Y. *et al.* Rich nature of Van Hove singularities in Kagome superconductor CsV_3Sb_5. *Nat. Commun.* **13**, 2220 (2022).

66. Kato, T. *et al.* Three-dimensional energy gap and origin of charge-density wave in kagome superconductor kv3sb5. *Commun. Mater.* **3**, 30, DOI: 10.1038/s43246-022-00255-1 (2022).

67. Ece, U., Ortiz, B. R., Wilson, S. D., Dressel, M. & Tsirlin, A. A. Optical detection of the density-wave instability in the kagome metal KV_3Sb_5. *NPJ Quantum Mater.* **7** (2022).

68. Uykur, E. *et al.* Low-energy optical properties of the nonmagnetic kagome metal CsV_3Sb_5. *Phys. Rev. B* **104**, 045130, DOI: 10.1103/PhysRevB.104.045130 (2021).

69. Wenzel, M. *et al.* Optical study of RbV_3Sb_5: Multiple density-wave gaps and phonon anomalies. *Phys. Rev. B* **105**, 245123, DOI: 10.1103/PhysRevB.105.245123 (2022).

70. Liang, Z. *et al.* Three-Dimensional Charge Density Wave and Surface-Dependent Vortex-Core States in a Kagome Superconductor CsV_3Sb_5. *Phys. Rev. X* **11**, 031026, DOI: 10.1103/PhysRevX.11.031026 (2021).

71. Huai, L. *et al.* Surface-induced orbital-selective band reconstruction in kagome superconductor CsV_3Sb_5. *Chin. Phys. B* **31**, 057403, DOI: 10.1088/1674-1056/ac4f50 (2022).

72. Nakayama, K. *et al.* Multiple energy scales and anisotropic energy gap in the charge-density-wave phase of the kagome superconductor csv_3sb_5. *Phys. Rev. B* **104**, L161112, DOI: 10.1103/PhysRevB.104.L161112 (2021).

73. LaBollita, H. & Botana, A. S. Tuning the Van Hove singularities in AV_3Sb_5 (A=K,Rb,Cs) via pressure and doping. *Phys. Rev. B* **104**, 205129, DOI: 10.1103/PhysRevB.104.205129 (2021).

74. Kautzsch, L. *et al.* Structural evolution of the kagome superconductors AV_3Sb_5 (A = K, Rb, and Cs) through charge density wave order. *Phys. Rev. Mater.* **7**, 024806, DOI: 10.1103/PhysRevMaterials.7.024806 (2023).

75. Luo, H. *et al.* Electronic nature of charge density wave and electron-phonon coupling in kagome superconductor KV_3Sb_5. *Nat. Commun.* **13**, 273, DOI: 10.1038/s41467-021-27946-6 (2022).

76. Kaboudvand, F., Teicher, S. M., Wilson, S. D., Seshadri, R. & Johannes, M. D. Fermi surface nesting and the Lindhard response function in the kagome superconductor CsV_3Sb_5. *Appl. Phys. Lett.* **120** (2022).

77. Xie, Y. *et al.* Electron-phonon coupling in the charge density wave state of CsV_3Sb_5. *Phys. Rev. B* **105**, L140501, DOI: 10.1103/PhysRevB.105.L140501 (2022).

78. Ferrari, F., Becca, F. & Valentí, R. Charge density waves in kagome-lattice extended Hubbard models at the Van Hove filling. *Phys. Rev. B* **106**, L081107, DOI: 10.1103/PhysRevB.106.L081107 (2022).

79. Wu, S. *et al.* Charge density wave order in the kagome metal AV_3Sb_5 (A=Cs,Rb,K). *Phys. Rev. B* **105**, 155106, DOI: 10.1103/PhysRevB.105.155106 (2022).

80. Azoury, D. *et al.* Direct observation of the collective modes of the charge density wave in the kagome metal csv₃sb₅. *Proc. Natl. Acad. Sci.* **120**, e2308588120, DOI: 10.1073/pnas.2308588120 (2023). https://www.pnas.org/doi/pdf/10.1073/pnas.2308588120.

81. Liu, G. *et al.* Observation of anomalous amplitude modes in the kagome metal csv3sb5. *Nat. Commun.* **13**, 3461, DOI: 10.1038/s41467-022-31162-1 (2022).

82. Jeong, M. Y. *et al.* Crucial role of out-of-plane Sb *p* orbitals in Van Hove singularity formation and electronic correlations in the superconducting kagome metal CsV_3Sb_5. *Phys. Rev. B* **105**, 235145, DOI: 10.1103/PhysRevB.105.235145 (2022).

83. Ritz, E. T., Fernandes, R. M. & Birol, T. Impact of Sb degrees of freedom on the charge density wave phase diagram of the kagome metal CsV_3Sb_5. *Phys. Rev. B* **107**, 205131, DOI: 10.1103/PhysRevB.107.205131 (2023).

84. Li, H., Liu, X., Kim, Y. B. & Kee, H.-Y. Origin of π-shifted three-dimensional charge density waves in the kagomé metal AV_3Sb_5 (A=Cs, Rb, K). *Phys. Rev. B* **108**, 075102, DOI: 10.1103/PhysRevB.108.075102 (2023).

85. Ortiz, B. R. *et al.* Fermi Surface Mapping and the Nature of Charge-Density-Wave Order in the Kagome Superconductor CsV_3Sb_5. *Phys. Rev. X* **11**, 041030, DOI: 10.1103/PhysRevX.11.041030 (2021).

86. Fu, Y. *et al.* Quantum Transport Evidence of Topological Band Structures of Kagome Superconductor CsV_3Sb_5. *Phys. Rev. Lett.* **127**, 207002, DOI: 10.1103/PhysRevLett.127.207002 (2021).

87. Shrestha, K. *et al.* Nontrivial Fermi surface topology of the kagome superconductor CsV_3Sb_5 probed by de Haas–van Alphen oscillations. *Phys. Rev. B* **105**, 024508, DOI: 10.1103/PhysRevB.105.024508 (2022).

88. Shrestha, K. *et al.* High quantum oscillation frequencies and nontrivial topology in kagome superconductor KV_3Sb_5 probed by torque magnetometry up to 45 T. *Phys. Rev. B* **107**, 155128, DOI: 10.1103/PhysRevB.107.155128 (2023).

89. Shrestha, K. *et al.* Fermi surface mapping of the kagome superconductor RbV_3Sb_5 using de Haas-van Alphen oscillations. *Phys. Rev. B* **107**, 075120, DOI: 10.1103/PhysRevB.107.075120 (2023).

90. Huang, X. *et al.* Three-dimensional fermi surfaces from charge order in layered csv_3sb_5. *Phys. Rev. B* **106**, 064510, DOI: 10.1103/PhysRevB.106.064510 (2022).

91. Broyles, C. *et al.* Effect of the Interlayer Ordering on the Fermi Surface of Kagome Superconductor CsV_3Sb_5 Revealed by Quantum Oscillations. *Phys. Rev. Lett.* **129**, 157001, DOI: 10.1103/PhysRevLett.129.157001 (2022).

92. Hu, Y. *et al.* Topological surface states and flat bands in the kagome superconductor CsV_3Sb_5. *Sci. Bull.* **67**, 495–500 (2022).

93. Fu, L. & Kane, C. L. Superconducting proximity effect and majorana fermions at the surface of a topological insulator. *Phys. Rev. Lett.* **100**, 096407, DOI: 10.1103/PhysRevLett.100.096407 (2008).

94. Li, H. *et al.* Observation of Unconventional Charge Density Wave without Acoustic Phonon Anomaly in Kagome Superconductors AV_3Sb_5 (A=Rb, Cs). *Phys. Rev. X* **11**, 031050, DOI: 10.1103/PhysRevX.11.031050 (2021).

95. Jiang, Y.-X. *et al.* Unconventional chiral charge order in kagome superconductor KV_3Sb_5. *Nat. Mater.* **20**, 1353–1357, DOI: 10.1038/s41563-021-01034-y (2021).

96. Zhao, H. *et al.* Cascade of correlated electron states in the kagome superconductor CsV_3Sb_5. *Nature* **599**, 216–221, DOI: 10.1038/s41586-021-03946-w (2021).

97. Shumiya, N. *et al.* Intrinsic nature of chiral charge order in the kagome superconductor RbV_3Sb_5. *Phys. Rev. B* **104**, 035131, DOI: 10.1103/PhysRevB.104.035131 (2021).

98. Christensen, M. H., Birol, T., Andersen, B. M. & Fernandes, R. M. Theory of the charge density wave in AV_3Sb_5 kagome metals. *Phys. Rev. B* **104**, 214513, DOI: 10.1103/PhysRevB.104.214513 (2021).

99. Subedi, A. Hexagonal-to-base-centered-orthorhombic $4Q$ charge density wave order in kagome metals KV_3Sb_5, RbV_3Sb_5 and CsV_3Sb_5. *Phys. Rev. Mater.* **6**, 015001, DOI: 10.1103/PhysRevMaterials.6.015001 (2022).

100. Frassineti, J. *et al.* Microscopic nature of the charge-density wave in the kagome superconductor RbV_3Sb_5. *Phys. Rev. Res.* **5**, L012017, DOI: 10.1103/PhysRevResearch.5.L012017 (2023).

101. Kang, M. *et al.* Charge order landscape and competition with superconductivity in kagome metals. *Nat. Mater.* **22**, 186–193, DOI: 10.1038/s41563-022-01375-2 (2023).

102. Hu, Y. *et al.* Coexistence of trihexagonal and star-of-David pattern in the charge density wave of the kagome superconductor AV_3Sb_5. *Phys. Rev. B* **106**, L241106, DOI: 10.1103/PhysRevB.106.L241106 (2022).

103. Stahl, Q. *et al.* Temperature-driven reorganization of electronic order in CsV_3Sb_5. *Phys. Rev. B* **105**, 195136, DOI: 10.1103/PhysRevB.105.195136 (2022).

104. Xiao, Q. *et al.* Coexistence of multiple stacking charge density waves in kagome superconductor CsV_3Sb_5. *Phys. Rev. Res.* **5**, L012032, DOI: 10.1103/PhysRevResearch.5.L012032 (2023).

105. Park, T., Ye, M. & Balents, L. Electronic instabilities of kagome metals: Saddle points and landau theory. *Phys. Rev. B* **104**, 035142, DOI: 10.1103/PhysRevB.104.035142 (2021).

106. Wang, Z. *et al.* Electronic nature of chiral charge order in the kagome superconductor CsV_3Sb_5. *Phys. Rev. B* **104**, 075148, DOI: 10.1103/PhysRevB.104.075148 (2021).

107. Li, H. *et al.* Rotation symmetry breaking in the normal state of a kagome superconductor KV_3Sb_5. *Nat. Phys.* **18**, 265–270, DOI: 10.1038/s41567-021-01479-7 (2022).

108. Li, H. *et al.* Unidirectional coherent quasiparticles in the high-temperature rotational symmetry broken phase of AV_3Sb_5 kagome superconductors. *Nat. Phys.* **19**, 637–643, DOI: 10.1038/s41567-022-01932-1 (2023).

109. Li, H. *et al.* No observation of chiral flux current in the topological kagome metal CsV_3Sb_5. *Phys. Rev. B* **105**, 045102, DOI: 10.1103/PhysRevB.105.045102 (2022).

110. Xu, Y. *et al.* Three-state nematicity and magneto-optical kerr effect in the charge density waves in kagome superconductors. *Nat. Phys.* **18**, 1470–1475, DOI: 10.1038/s41567-022-01805-7 (2022).

111. Saykin, D. R. *et al.* High Resolution Polar Kerr Effect Studies of CsV_3Sb_5: Tests for Time-Reversal Symmetry Breaking below the Charge-Order Transition. *Phys. Rev. Lett.* **131**, 016901, DOI: 10.1103/PhysRevLett.131.016901 (2023).

112. Chen, D. *et al.* Anomalous thermoelectric effects and quantum oscillations in the kagome metal CsV_3Sb_5. *Phys. Rev. B* **105**, L201109, DOI: 10.1103/PhysRevB.105.L201109 (2022).

113. Khasanov, R. *et al.* Time-reversal symmetry broken by charge order in CsV_3Sb_5. *Phys. Rev. Res.* **4**, 023244, DOI: 10.1103/PhysRevResearch.4.023244 (2022).

114. Guo, C. *et al.* Switchable chiral transport in charge-ordered kagome metal CsV_3Sb_5. *Nature* **611**, 461–466, DOI: 10.1038/s41586-022-05127-9 (2022).

115. Nie, L. *et al.* Charge-density-wave-driven electronic nematicity in a kagome superconductor. *Nature* **604**, 59–64, DOI: 10.1038/s41586-022-04493-8 (2022).

116. Luo, J. *et al.* Possible star-of-David pattern charge density wave with additional modulation in the kagome superconductor CsV_3Sb_5. *npj Quantum Mater.* **7**, 30, DOI: 10.1038/s41535-022-00437-7 (2022).

117. Song, D. *et al.* Orbital ordering and fluctuations in a kagome superconductor CsV_3Sb_5. *Sci. China Physics, Mech. & Astron.* **65**, 247462, DOI: 10.1007/s11433-021-1826-1 (2022).

118. Wulferding, D. *et al.* Emergent nematicity and intrinsic versus extrinsic electronic scattering processes in the kagome metal CsV_3Sb_5. *Phys. Rev. Res.* **4**, 023215, DOI: 10.1103/PhysRevResearch.4.023215 (2022).

119. Ratcliff, N., Hallett, L., Ortiz, B. R., Wilson, S. D. & Harter, J. W. Coherent phonon spectroscopy and interlayer modulation of charge density wave order in the kagome metal CsV_3Sb_5. *Phys. Rev. Mater.* **5**, L111801, DOI: 10.1103/PhysRevMaterials.5.L111801 (2021).

120. Yu, F. H. *et al.* Concurrence of anomalous hall effect and charge density wave in a superconducting topological kagome metal. *Phys. Rev. B* **104**, L041103, DOI: 10.1103/PhysRevB.104.L041103 (2021).

121. Guguchia, Z. *et al.* Tunable unconventional kagome superconductivity in charge ordered RbV_3Sb_5 and KV_3Sb_5. *Nat. Commun.* **14**, 153, DOI: 10.1038/s41467-022-35718-z (2023).

122. Wang, L. *et al.* Anomalous Hall effect and two-dimensional Fermi surfaces in the charge-density-wave state of kagome metal RbV_3Sb_5. *J. Physics: Mater.* **6**, 02LT01, DOI: 10.1088/2515-7639/acba46 (2023).

123. Mielke, C. *et al.* Time-reversal symmetry-breaking charge order in a kagome superconductor. *Nature* **602**, 245–250, DOI: 10.1038/s41586-021-04327-z (2022).

124. Yang, S.-Y. *et al.* Giant, unconventional anomalous Hall effect in the metallic frustrated magnet candidate, KV_3Sb_5. *Sci. Adv.* **6**, eabb6003, DOI: 10.1126/sciadv.abb6003 (2020). https://www.science.org/doi/pdf/10.1126/sciadv.abb6003.

125. Yu, L. *et al.* Evidence of a hidden flux phase in the topological kagome metal CsV_3Sb_5. *arXiv:2107.10714* (2021).

126. Shan, Z. *et al.* Muon spin relaxation study of the layered kagome superconductor csv$_3$sb$_5$. *Phys. Rev. Res.* **4**, 033145, DOI: 10.1103/PhysRevResearch.4.033145 (2022).

127. Asaba, T. *et al.* Evidence for an odd-parity nematic phase above the charge density wave transition in kagome metal CsV_3Sb_5 (2023). 2309.16985.

128. Subires, D. *et al.* Order-disorder charge density wave instability in the kagome metal (Cs,Rb)V_3Sb_5. *Nat. Commun.* **14**, 1015, DOI: 10.1038/s41467-023-36668-w (2023).

129. Chen, Q., Chen, D., Schnelle, W., Felser, C. & Gaulin, B. D. Charge Density Wave Order and Fluctuations above T_{CDW} and below Superconducting T_c in the Kagome Metal CsV_3Sb_5. *Phys. Rev. Lett.* **129**, 056401, DOI: 10.1103/PhysRevLett.129.056401 (2022).

130. Zhu, C. C. *et al.* Double-dome superconductivity under pressure in the V-based kagome metals AV_3Sb_5 (A=Rb and K). *Phys. Rev. B* **105**, 094507, DOI: 10.1103/PhysRevB.105.094507 (2022).

131. Zhou, S. & Wang, Z. Chern fermi pocket, topological pair density wave, and charge-4e and charge-6e superconductivity in kagomé superconductors. *Nat. Commun.* **13**, 7288, DOI: 10.1038/s41467-022-34832-2 (2022).

132. Li, H. *et al.* Small fermi pockets intertwined with charge stripes and pair density wave order in a kagome superconductor. *Phys. Rev. X* **13**, 031030, DOI: 10.1103/PhysRevX.13.031030 (2023).

133. Yin, Q. *et al.* Superconductivity and Normal-State Properties of Kagome Metal RbV_3Sb_5 Single Crystals. *Chin. Phys. Lett.* **38**, 037403, DOI: 10.1088/0256-307X/38/3/037403 (2021).

134. Ortiz, B. R. *et al.* Superconductivity in the Z2 kagome metal KV_3Sb_5. *Phys. Rev. Mater.* **5**, 034801, DOI: 10.1103/PhysRevMaterials.5.034801 (2021).

135. Duan, W. *et al.* Nodeless superconductivity in the kagome metal CsV_3Sb_5. *Sci. China Physics, Mech. & Astron.* **64**, 107462, DOI: 10.1007/s11433-021-1747-7 (2021).

136. Ni, S. *et al.* Anisotropic Superconducting Properties of Kagome Metal CsV_3Sb_5. *Chin. Phys. Lett.* **38**, 057403, DOI: 10.1088/0256-307X/38/5/057403 (2021).

137. Zhong, Y. *et al.* Nodeless electron pairing in CsV_3Sb_5-derived kagome superconductors. *Nature* **617**, 488–492, DOI: 10.1038/s41586-023-05907-x (2023).

138. Roppongi, M. *et al.* Bulk evidence of anisotropic s-wave pairing with no sign change in the kagome superconductor CsV_3Sb_5. *Nat. Commun.* **14**, 667, DOI: 10.1038/s41467-023-36273-x (2023).

139. Mu, C. *et al.* S-Wave Superconductivity in Kagome Metal CsV_3Sb_5 Revealed by 121/123Sb NQR and 51V NMR Measurements. *Chin. Phys. Lett.* **38**, 077402, DOI: 10.1088/0256-307X/38/7/077402 (2021).

140. Yin, L. *et al.* Strain-sensitive superconductivity in the kagome metals KV_3Sb_5 and CsV_3Sb_5 probed by point-contact spectroscopy. *Phys. Rev. B* **104**, 174507, DOI: 10.1103/PhysRevB.104.174507 (2021).

141. Gupta, R. *et al.* Microscopic evidence for anisotropic multigap superconductivity in the CsV_3Sb_5 kagome superconductor. *npj Quantum Mater.* **7**, 49, DOI: 10.1038/s41535-022-00453-7 (2022).

142. Holbæk, S. C., Christensen, M. H., Kreisel, A. & Andersen, B. M. Unconventional superconductivity protected from disorder on the kagome lattice. *Phys. Rev. B* **108**, 144508, DOI: 10.1103/PhysRevB.108.144508 (2023).

143. Zhang, X. *et al.* Vortex phase diagram of kagome superconductor CsV_3Sb_5 (2023). 2306.13297.

144. Varma, C. M. & Wang, Z. Extended superconducting fluctuation region and 6e and 4e flux-quantization in a Kagome compound with a normal state of 3Q-order (2023). 2307.00448.

145. Ge, J. *et al.* Discovery of charge-4e and charge-6e superconductivity in kagome superconductor CsV_3Sb_5. *arXiv:2201.10352* (2022).

146. Chen, K. Y. *et al.* Double Superconducting Dome and Triple Enhancement of T_c in the Kagome Superconductor CsV_3Sb_5 under High Pressure. *Phys. Rev. Lett.* **126**, 247001, DOI: 10.1103/PhysRevLett.126.247001 (2021).

147. Wang, N. N. *et al.* Competition between charge-density-wave and superconductivity in the kagome metal RbV_3Sb_5. *Phys. Rev. Res.* **3**, 043018, DOI: 10.1103/PhysRevResearch.3.043018 (2021).

148. Du, F. *et al.* Pressure-induced double superconducting domes and charge instability in the kagome metal KV_3Sb_5. *Phys. Rev. B* **103**, L220504, DOI: 10.1103/PhysRevB.103.L220504 (2021).

149. Oey, Y. M. *et al.* Fermi level tuning and double-dome superconductivity in the kagome metal $CsV_3Sb_{5-x}Sn_x$. *Phys. Rev. Mater.* **6**, L041801, DOI: 10.1103/PhysRevMaterials.6.L041801 (2022).

150. Oey, Y. M., Kaboudvand, F., Ortiz, B. R., Seshadri, R. & Wilson, S. D. Tuning charge density wave order and superconductivity in the kagome metals $KV_3Sb_{5-x}Sn_x$ and $RbV_3Sb_{5-x}Sn_x$. *Phys. Rev. Mater.* **6**, 074802, DOI: 10.1103/PhysRevMaterials.6.074802 (2022).

151. Yu, F. H. *et al.* Unusual competition of superconductivity and charge-density-wave state in a compressed topological kagome metal. *Nat. Commun.* **12**, 3645, DOI: 10.1038/s41467-021-23928-w (2021).

152. Tsirlin, A. A. *et al.* Effect of nonhydrostatic pressure on the superconducting kagome metal CsV_3Sb_5. *Phys. Rev. B* **107**, 174107, DOI: 10.1103/PhysRevB.107.174107 (2023).

153. Feng, X. Y. *et al.* Commensurate-to-incommensurate transition of charge-density-wave order and a possible quantum critical point in pressurized kagome metal CsV_3Sb_5. *npj Quantum Mater.* **8**, 23, DOI: 10.1038/s41535-023-00555-w (2023).

154. Zheng, L. *et al.* Emergent charge order in pressurized kagome superconductor CsV_3Sb_5. *Nature* **611**, 682–687, DOI: 10.1038/s41586-022-05351-3 (2022).

155. Sur, Y., Kim, K.-T., Kim, S. & Kim, K. H. Optimized superconductivity in the vicinity of a nematic quantum critical point in the kagome superconductor $Cs(V_{1-x}Ti_x)_3Sb_5$. *Nat. Commun.* **14**, 3899, DOI: 10.1038/s41467-023-39495-1 (2023).

156. Yang, H. *et al.* Titanium doped kagome superconductor $CsV_{3-x}Ti_xSb_5$ and two distinct phases. *Sci. Bull.* **67**, 2176–2185 (2022).

157. Kautzsch, L. *et al.* Incommensurate charge-stripe correlations in the kagome superconductor $CsV_3Sb_{5-x}Sn_x$. *npj Quantum Mater.* **8**, 37, DOI: 10.1038/s41535-023-00570-x (2023).

158. Li, H. *et al.* Discovery of conjoined charge density waves in the kagome superconductor CsV_3Sb_5. *Nat. Commun.* **13**, 6348, DOI: 10.1038/s41467-022-33995-2 (2022).

159. Ortiz, B. R. *et al.* Complete miscibility amongst the AV_3Sb_5 kagome superconductors: Design of mixed A-site AV_3Sb_5 (A: K, Rb, Cs) alloys. *Phys. Rev. Mater.* **7**, 014801 (2023).

160. Liu, M. *et al.* Evolution of superconductivity and charge density wave through Ta and Mo doping in CsV_3Sb_5. *Phys. Rev. B* **106**, L140501 (2022).

161. Li, Y. *et al.* Tuning the competition between superconductivity and charge order in the kagome superconductor $Cs(V_{1-x}Nb_x)_3Sb_5$. *Phys. Rev. B* **105**, L180507 (2022).

162. Zhou, X. *et al.* Effects of niobium doping on the charge density wave and electronic correlations in the kagome metal $Cs(V_{1-x}Nb_x)_3Sb_5$. *Phys. Rev. B* **107**, 125124 (2023).

163. Xiao, Q. *et al.* Evolution of charge density waves from three-dimensional to quasi-two-dimensional in Kagome superconductors $Cs(V_{1-x}M_x)_3Sb_5$ (M = Nb, Ta). *arXiv:2304.01740* (2023).

164. Li, J. *et al.* Strong-coupling superconductivity and weak vortex pinning in Ta-doped CsV_3Sb_5 single crystals. *Phys. Rev. B* **106**, 214529 (2022).

165. Liu, Y. *et al.* Doping evolution of superconductivity, charge order, and band topology in hole-doped topological kagome superconductors Cs $(V_{1-x}Ti_x)_3Sb_5$. *Phys. Rev. Mater.* **7**, 064801 (2023).

166. Hou, J. *et al.* Effect of hydrostatic pressure on the unconventional charge density wave and superconducting properties in two distinct phases of doped kagome superconductors $CsV_{3-x}Ti_xSb_5$. *Phys. Rev. B* **107**, 144502 (2023).

167. Ding, G., Wo, H., Gu, Y., Gu, Y. & Zhao, J. Effect of chromium doping on superconductivity and charge density wave order in the kagome metal $Cs(V_{1-x}Cr_x)_3Sb_5$. *Phys. Rev. B* **106**, 235151 (2022).

168. Liu, Y. *et al.* Enhancement of superconductivity and suppression of charge-density wave in As-doped CsV_3Sb_5. *Phys. Rev. Mater.* **6**, 124803 (2022).

169. Capa Salinas, A. N. *et al.* Electron-hole asymmetry in the phase diagram of carrier-tuned CsV_3Sb_5. *Front. Electron. Mater.* **3**, 1257490 (2023).

170. Oey, Y. M. *et al.* Fermi level tuning and double-dome superconductivity in the kagome metal $CsV_3Sb_{5-x}Sn_x$. *Phys. Rev. Mater.* **6**, L041801 (2022).

171. Lei, X. *et al.* Band splitting and enhanced charge density wave modulation in Mn-implanted CsV_3Sb_5. *Nanoscale Adv.* **5**, 2785–2793 (2023).

172. Werhahn, D. *et al.* The kagomé metals $RbTi_3Bi_5$ and $CsTi_3Bi_5$. *Zeitschrift für Naturforschung B* **77**, 757–764 (2022).

173. Liu, B. *et al.* Tunable Van Hove Singularity without Structural Instability in Kagome Metal $CsTi_3Bi_5$. *Phys. Rev. Lett.* **131**, 026701, DOI: 10.1103/PhysRevLett.131.026701 (2023).

174. Wang, Y. *et al.* Flat Band and Z2 Topology of Kagome Metal $CsTi_3Bi_5$. *Chin. Phys. Lett.* **40**, 037102, DOI: 10.1088/0256-307X/40/3/037102 (2023).

175. Li, H. *et al.* Electronic nematicity without charge density waves in titanium-based kagome metal. *Nat. Phys.* 1–8 (2023).

176. Yang, H. *et al.* Titanium-based kagome superconductor $CsTi_3Bi_5$ and topological states (2022). 2209.03840.

177. Liu, Y. *et al.* Superconductivity emerged from density-wave order in a kagome bad metal. *arXiv:2309.13514* (2023).

178. Pokharel, G. *et al.* Electronic properties of the topological kagome metals YV_6Sn_6 and GdV_6Sn_6. *Phys. Rev. B* **104**, 235139, DOI: 10.1103/PhysRevB.104.235139 (2021).

179. Ishikawa, H., Yajima, T., Kawamura, M., Mitamura, H. & Kindo, K. GdV_6Sn_6: A Multi-carrier Metal with Non-magnetic 3d-electron Kagome Bands and 4f-electron Magnetism. *J. Phys. Soc. Jpn.* **90**, 124704, DOI: 10.7566/JPSJ.90.124704 (2021). https://doi.org/10.7566/JPSJ.90.124704.

180. Qian, T. *et al.* Revealing the competition between charge density wave and superconductivity in CsV_3Sb_5 through uniaxial strain. *Phys. Rev. B* **104**, 144506, DOI: 10.1103/PhysRevB.104.144506 (2021).

181. Guo, C. *et al.* Correlated order at the tipping point in the kagome metal CsV_3Sb_5 (2023). 2304.00972.

182. Xing, Y. *et al.* Optical Manipulation of the Charge Density Wave state in RbV_3Sb_5 (2023). 2308.04128.

183. Christensen, M. H., Birol, T., Andersen, B. M. & Fernandes, R. M. Loop currents in AV_3Sb_5 kagome metals: Multipolar and toroidal magnetic orders. *Phys. Rev. B* **106**, 144504, DOI: 10.1103/PhysRevB.106.144504 (2022).

Highlighted References

Ortiz, B. R. et al. New kagome prototype materials: discovery of KV_3Sb_5, RbV_3Sb_5, and CsV_3Sb_5. Phys. Rev. Mater. 3, 094407 (2019).
This 2019 paper by Ortiz et al. reports the discovery of the AV_3Sb_5 structure type and an initial measurements of their physical properties.

Ortiz, B. R. et al. CsV_3Sb_5: A Z2 Topological Kagome Metal with a Superconducting Ground State. Phys. Rev. Lett. 125, 247002 (2020).
This 2020 paper by Ortiz et al. reports the discovery of superconductivity in the AV_3Sb_5 class of materials as well as the identification of a charge density wave-like anomaly at high temperature.

Jiang, Y.-X. et al. Unconventional chiral charge order in kagome superconductor KV_3Sb_5. Nat. Mater. 20, 1353–1357 (2021).
Jiang et al. is an STM study reporting the real space visualization of charge density wave order in KV_3Sb_5 and an observation of the CDW state coupling to an external magnetic field.

Zhao, H. et al. Cascade of correlated electron states in the kagome superconductor CsV_3Sb_5. Nature 599, 216–221(2021).
Zhao et al. is an STM study reporting the visualization of CDW order in CsV_3Sb_5 as well as the staged evolution of charge order upon cooling, reporting the observation of quasi-1D charge stripes below an intermediate temperature scale.

Chen, H. et al. Roton pair density wave in a strong-coupling kagome superconductor. Nature 599, 222–228 (2021).
Chen et al. is a low-temperature STM study reporting the formation of an additional 3q charger ordering wave vector that couples to and modulates the superfluid density.

Xu, Y. et al. Three-state nematicity and magneto-optical Kerr effect in the charge density waves in kagome superconductors. Nat. Phys. 18, 1470–1475 (2022).
Xu et al. is an optical study that reports the formation of orthorhombic, structural twin domains as well as chiral/TRS-broken subdomains below the CDW transition across the AV_3Sb_5 family of compounds.

Kang, M. et al. Twofold van Hove singularity and origin of charge order in topological kagome superconductor CsV_3Sb_5. Nat. Phys. 18, 301–308 (2022).
Kang et al. is an ARPES study that identifies the presence of multiple VHS near E_F in CsV_3Sb_5 and explores the coupling of these states to the onset of CDW order.

Mielke, C. et al. Time-reversal symmetry-breaking charge order in a kagome superconductor. Nature 602, 245–250, DOI: 10.1038/s41586-021-04327-z (2022).
Mielke et al. is a μSR study that reports broken TRS below the CDW transition in KV_3Sb_5.

Guo, C. et al. Switchable chiral transport in charge-ordered kagome metal CsV_3Sb_5. Nature 611, 461–466(2022). *Guo et al. is a magnetotransport study that reports field-switchable chiral transport effects at low-temperature in CsV_5Sb_5, suggestive of structural chirality or broken TRS.*

Yang, S.-Y. et al. Giant, unconventional anomalous Hall effect in the metallic frustrated magnet candidate, KV3Sb5. Sci. Adv. 6, eabb6003 (2020). *Yang et al. is a magnetotransport study that reports an unusually large anamalous Hall effect in the CDW state of KV_3Sb_5.*

Acknowledgements

S.D.W. gratefully acknowledges support from the UC Santa Barbara NSF Quantum Foundry funded via the Q-AMASE-i program under award DMR-1906325 and the Eddleman Center for Quantum Innovation. B.R.O gratefully acknowledges support from the U.S. Department of Energy (DOE), Office of Science, Basic Energy Sciences (BES), Materials Sciences and Engineering Division.

Competing interests

S.D.W. and B.R.O. declare no competing financial interests in creating this work. Notice: This manuscript has been authored by UT-Battelle, LLC under Contract No. DE-AC05-00OR22725 with the U.S. Department of Energy. The United States Government retains and the publisher, by accepting the article for publication, acknowledges that the United States Government retains a non-exclusive, paid-up, irrevocable, world-wide license to publish or reproduce the published form of this manuscript, or allow others to do so, for United States Government purposes. The Department of Energy will provide public access to these results of federally sponsored research in accordance with the DOE Public Access Plan (http://energy.gov/downloads/doe-public-access-plan).

Figure Captions

Figure 1: Crystal and electronic band structures of AV_3Sb_5 compounds a | Lattice structure of AV_3Sb_5 with A=K, Rb, Cs. Red spheres show the kagome net of V atoms, each coordinated by an octahedra of Sb atoms depicted as gold spheres. Between the V_3Sb_5 layers is a honeycomb lattice of alkali metal A-site atoms, depicted as blue spheres. b | The electronic band structure of AV_3Sb_5 determined via density functional theory calculations. Key features native to the kagome network are highlighted in the $k_z = 0$ plane such as a series of two saddle points with V orbital character just below E_F at the M-point, V-based Dirac points below E_F at the K-point, and a mixed (V,Sb) character saddle point above E_F at the M-point. A representative Brillouin zone (BZ) is also illustrated with the location of high-symmetry points labeled.

Figure 2: Elements of CDW order in AV_3Sb_5 compounds. The structure of CDW order in AV_3Sb_5 can be thought of a combination of a several key elements. The first element is the primary component of the real order parameter and is the in-plane 3**q** distortion of the kagome plane, which is favored as breathing into SoD or TrH-type distortions. The second element is the proposed imaginary component, which modulates hopping into an orbital flux phase and breaks TRS. The third element is the interplane correlation that modulates the real component of the CDW state along the c-axis. This arises via consideration of out-of-plane momenta (along the L-points) that modulate the phasing or distortion types between the planes. RbV_3Sb_5 and KV_3Sb_5 each show a TrH in-plane distortion that is staggered by half an in-plane lattice constant along the c-axis. CsV_3Sb_5 has a mixed-phase CDW, whose average 4-layer structure refines to a mixture of staggered TrH distortion interwoven with staggered TrH and SoD distorted layers.

Figure 3: Intermediate electronic phase transitions and crossovers in AV_3Sb_5. The progression of phase transitions and reports of symmetry lowering, such as time reversal symmetry breaking (TRSB), in AV_3Sb_5 compounds. Reports of lattice and electronic anomalies are visually depicted here and described further in the text. The range of reported residual resistivity ratios ($RRR \equiv \rho_{4K}/\rho_{300K}$) for each compound is summarized next to each chart of anomalies. The majority of anomalies intermediate between the onset of CDW order and SC are currently reported in CsV_3Sb_5. Data for CsV_3Sb_5 are drawn from PDW[26], ANE[112], Modified TRSB (μSR)[113], Chiral/TRSB (transport)[114], 1D quasiparticles (STM)[108], Nematic (elastoresistance)[115], Modified CDW (NMR)[116], $T^{-1}T$ anomaly (NMR)[117], $4a_0$ stripes (STM)[96], Lattice anomaly (Raman)[79,118], Lattice anomaly (TR-OR)[119], AHE[120], TRSB (CD)[110], and TRSB (μSR)[116]. Data for RbV_3Sb_5 are drawn from TRSB (CD)[110], TRSB (μSR)[121], AHE[122], and modified TRSB (μSR)[121]. Data for KV_3Sb_5 are drawn from TRSB (CD)[110], TRSB (μSR)[123], AHE[124], and modified TRSB (μSR)[123].

Figure 4: Schematic of momentum space contours of the Fermi surface and corresponding nesting wave vectors for electronic order. a | Nesting wave vectors in the unfolded and folded BZ above and below the CDW transition respectively. Nested M-points are illustrated in the unfolded zone while a schematic of nested Chern pockets are highlighted in the folded zone, below T_{CDW}. b | Wave vectors of charge correlations resolved within the ab-plane as reported via STM measurements and a tabulation of compounds where these correlations have been reported.

Figure 5: Doping and pressure-tuned phase diagrams of AV_3Sb_5 compounds. a | Pressure-Temperature electronic phase diagram showing the evolution of CDW and SC orders as a function of normalized pressure. The pressure value is normalized by the critical pressure P_c where the CDW state is reported to vanish. b | Electronic phase diagram as a function of normalized hole-doping. Doping concentrations have been normalized by the critical hole-doping value x_c where CDW order nominally vanishes. CDW transition temperatures have been normalized relative to their undoped, ambient pressure values of 100%. Data were adapted from[146–150].

Figure 6: Schematic showing sublattice doping of CsV_3Sb_5 with various electronic, magnetic, and isoelectronic dopants. Percent substitution achievable for dopants on each site of CsV_3Sb_5 and their influence on T_{CDW} and T_c are illustrated. Data are extracted from[156,159–171]

Short summary

This article reviews the experimental and theoretical pictures of the fascinating class of AV_3Sb_5 kagome metals. The properties of their anomalous charge density wave and superconducting are reviewed, and future directions for studying these and related kagome metals are discussed.